Biomicrofluidics

Field enhancement in microfluidic semiconductor nanowire array

Cite as: Biomicrofluidics **14**, 064102 (2020); https://doi.org/10.1063/5.0028899
Submitted: 08 September 2020 . Accepted: 15 October 2020 . Published Online: 02 November 2020

Bhamy Maithry Shenoy, Gopalkrishna Hegde, and D. Roy Mahapatra

Biomicrofluidics ARTICLE scitation.org/journal/bmf

Field enhancement in microfluidic semiconductor nanowire array

Cite as: Biomicrofluidics 14, 064102 (2020); doi: 10.1063/5.0028899
Submitted: 8 September 2020 · Accepted: 15 October 2020 ·
Published Online: 2 November 2020

Bhamy Maithry Shenoy,[1] Gopalkrishna Hegde,[2] and D. Roy Mahapatra[1,a)]

AFFILIATIONS

[1]Department of Aerospace Engineering, Indian Institute of Science, Bangalore 560012, India
[2]BioSystems Science and Engineering, Indian Institute of Science, Bangalore 560012, India

[a)]**Author to whom correspondence should be addressed:** roymahapatra@iisc.ac.in

ABSTRACT

Nano-material integrated microfluidic platforms are increasingly being considered to accelerate biological sample preparation and molecular diagnostics. A major challenge in this context is the generation of high electric fields for electroporation of cell membranes. In this paper, we have studied a novel mechanism of generating a high electric field in the microfluidic channels by using an array of semiconductor nanowires. When an electrostatic field is applied across a semiconductor nanowire array, the electric field is localized near the nanowires and the field strength is higher than what was reported previously with various other micro-geometries. Nanowires made of ZnO, Si, and Si–SiO_2 and their orientation and array spacing are considered design parameters. It is observed that for a given ratio of the spacing between nanowires to the diameter, the electric field enhancement near the edges of ZnO nanowires is nearly 30 times higher compared to Si or Si–SiO_2 nanowire arrays. This enhancement is a combined effect of the unique geometry with a pointed tip with a hexagonal cross section, the piezoelectric and the spontaneous polarization in the ZnO nanowires, and the electro-kinetics of the interface fluid. Considering the field localization phenomena, the trajectories of *E. coli* cells in the channel are analyzed. For a given inter-nanowire spacing and an applied electric field, the channels with ZnO nanowire arrays have a greater probability of cell lysis in comparison to Si-based nanowire arrays. Detailed correlations between the cell lysis probability with the inter-nanowire spacing and the applied electric field are reported.

I. INTRODUCTION

Microfluidic lab-on-chip (LOC) devices have attracted significant attention in recent years due to the lower cost of mass production, high efficiency, portability, and small sample volumes. Lysis is essential for the analysis of intracellular components and similar constituents from bacteria and viruses. Cell lysis can be accomplished using chemical,[1–3] mechanical,[4–6] thermal,[7–9] optical,[10,11] or electrical methods.[12–18] To have the ability to integrate with a complex LOC device, the lysis technique should be universal to the type and property of the sample and should not interfere with subsequent bioassays. Chemical methods require lytic reagents such as sodium dodecyl sulfate[3] that may interfere with downstream analysis. Mechanical methods have high efficiency, but the lysate is homogenized in the process and hence not suitable for organelle discrimination. Thermal methods disrupt cell membranes at high temperatures and are not suitable for studying protein molecules as they denature when heated. Optical methods require an elaborate setup. In contrast, electrical lysis uses an electric field for cell lysis, which is relatively easy to implement and does not affect downstream analysis. However, effective electrical lysis of cells in such devices present several challenges such as the generation of high electric fields at low voltages without causing electrolysis of flowing solution, optimal geometry to avoid cell clogging and heat generation, optimal fields so that the intracellular components are not affected, effective cell sorting, optimal fluid flow rates, etc. A microdevice for electrical cell lysis was first designed by Lee *et al.*[18] High density of sharp Cr/Au microelectrodes with 5 μm separation was used for concentration of electric fields, and lysis was accomplished using AC or DC electric fields. To avoid bubble formation at the electrodes due to high fields, a combination of AC and DC fields were used by many groups[14,19] for electrical lysis. Another design used special geometry to enhance electric field locally in previously destined regions of a microfluidic channel.[15,17,20] Large metal electrodes patterned at the bottom positioned perpendicularly to the main channel were used in the combination of AC field for electrical lysis.[13] Other research groups have used lower electric fields in

combination of hypotonic detergent containing high or low pH buffers to lyse the cells.[21–23]

The electrical lysis of cells is based on electroporation of the cell membrane. The cell membrane is a dielectric phospholipid bi-layered structure, which is permeable to selective ions through ion channels. When an external electric field is applied, the phospholipid layer is deformed and pores are formed thereby increasing the permeability of the cell membrane. However, since the electrical current density in the cytoplasm is less than that in the surrounding fluid, electric potential change occurs in the cytoplasm at a slower rate than in the extracellular space. The difference in the potential between the extracellular space and in the cytoplasm results in a voltage drop across the cell membrane. This imposed transmembrane potential depends on the size and orientation of the cell, structure, and material of the cell membrane and magnitude of the applied electric field. At a sufficiently high field, greater than a critical value, the transmembrane potential increases, and the size of pores on the cell membrane increases due to swelling of cells by electroporation and structure degradation of membrane proteins. These pores may seal spontaneously or remain open indefinitely. The coalescence of many stable pores then leads to the fracture of the cell membrane. The detailed mechanism can be found in the literature.[24]

The emergence of semiconductor nanostructures integrated with microfluidic devices is a natural progression into the next generation of LOC devices. Their wide range of applications has proliferated into numerous areas such as sensing of proteins,[25] tumors,[26–29] immunoglobulins,[30] disease diagnostics,[31] single-cell mapping,[32] energy harvesting,[33] manipulation, characterization[34,35] and mechanical lysing of biological cells,[36] and so on. Nanowire arrays are increasingly being used in manipulation, transportation, sensing, etc., of biomolecules. Zheng *et al.* reported interesting designs of electrodes such as copper nanowires grown on a copper foam structure[37] and carbon nanotube (CNT) sponge[38] for inactivation of virus and bacteria (*E. coli*) from water at low voltage. They used a simplified estimation of field enhancement and the resulting impact on *E. coli* particles.[39]

In this paper, we propose a novel method of amplifying the electric field at low voltage using an array of semiconductor nanowires in the microfluidic channel. Due to the difference in the dielectric permittivity of the nanostructure material from the surrounding fluid medium, the electric field localizes near the nanostructures. This results in a non-uniform field in the channel. This can be used for lysing and electro-kinetic transport in the microfluidic channel. In the present paper, we investigate the effect of geometry, inter-nanowire spacing, and orientation on the electric field enhancement in the microfluidic channels with vertical nanowire arrays of Si, SiO_2 coated Si, and ZnO nanowires. Electro-mechanical coupling interactions in semiconductor nanostructure along with the diffusive and electro-kinetic migration of ions in the fluid are taken into account. ZnO nanowires can be grown with pointed tips similar to the microelectrodes in earlier designs and possess several useful properties like spontaneous polarization, piezoelectricity, biocompatibility, and chemical sensitivity. Besides, ZnO nanowires have recently been fabricated *in situ* in the microfluidic channel by hydrothermal reaction,[40] and its growth mechanism has been confirmed.[41] Si nanowires have the advantage of well-established fabrication technologies that can be adopted for device integration. We further analyze the effect of non-uniform electric field distribution in the channel on the trajectories of biological cells. We define a probability of lysis factor to estimate the efficiency of the channels in lysing bacterial cells. The effects of inter-nanowire spacings and the applied electric fields on *E. coli* cell lysis are analyzed.

II. MATHEMATICAL MODEL

We propose a multiphysics model to analyze the electric field distribution in microfluidic channels consisting of the semiconductor nanowire array. The formulation consistently takes into account the effect of electro-mechanical coupling in semiconductor nanowires with the diffusion and electro-kinetic motion of ions in the fluid medium. The effect of nanowire geometry, orientation to the applied electric field, and the inter-nanowire spacing are analyzed.

A. Electric field distribution in the microfluidic channel due to semiconductor nanostructures

The micro-channel configuration considered for the present simulation is defined by the length (d_0), width (w_0), and height (h_0) as shown in Fig. 1. An array of nanowires are considered on the channel bed such that it makes a continuous row of closely placed nanowires in x and y directions. The nanowires are assumed to have the same dimensions with diameter d_n, height h_n, and the inter-nanowire spacing d_s. An electrolytic solution is present in the microfluidic channel.

When an electric field is applied across an array of semiconductor nanowires in a fluid medium, the field distribution is influenced by the difference in dielectric permittivity and conductivity (or resistivity) of different media. At the solid/fluid junction, there is charge transfer from the fluid to the semiconductor, conduction in the semiconductor, and charge transfer from the semiconductor to the fluid region depending upon the energies of conduction and valence bands and the electrolyte species. Also, for closely packed nanowires, there are inter-nanowire interactions. Quantum mechanical tunneling is also important in the nano-regime. For intrinsic semiconductors at low voltages as in the present case, the carrier concentration is low and hence electric conduction is small. For such cases, the electric field distribution in the channel due to an electric field applied across a nanowire array made up of piezoelectric semiconductor depends on the electrical permittivity of the semiconductor and the fluid medium and is governed by Maxwell's equation for electrostatics, that is,

$$\nabla \cdot D = \begin{cases} \rho_f, & D = \epsilon E \text{ in } \Omega_f, \\ \rho_s, & D = \epsilon E + e\varepsilon + P_{sp} \text{ in } \Omega_s, \end{cases} \tag{1}$$

where D, ϵ, E, ε, e, and P_{sp} are the electric displacement vector, the dielectric permittivity tensor, electric field, strain tensor, the piezoelectric tensor, and the spontaneous polarization, respectively. Ω_s and Ω_f denote the semiconductor and fluid domains, respectively. The second and third terms in Ω_s are due to piezoelectric and spontaneous polarization in the semiconductor nanostructure. ρ_f is the charge density due to ions in the fluid domain (Ω_f) and ρ_s is the charge density due to electrons, holes, and dopants in the

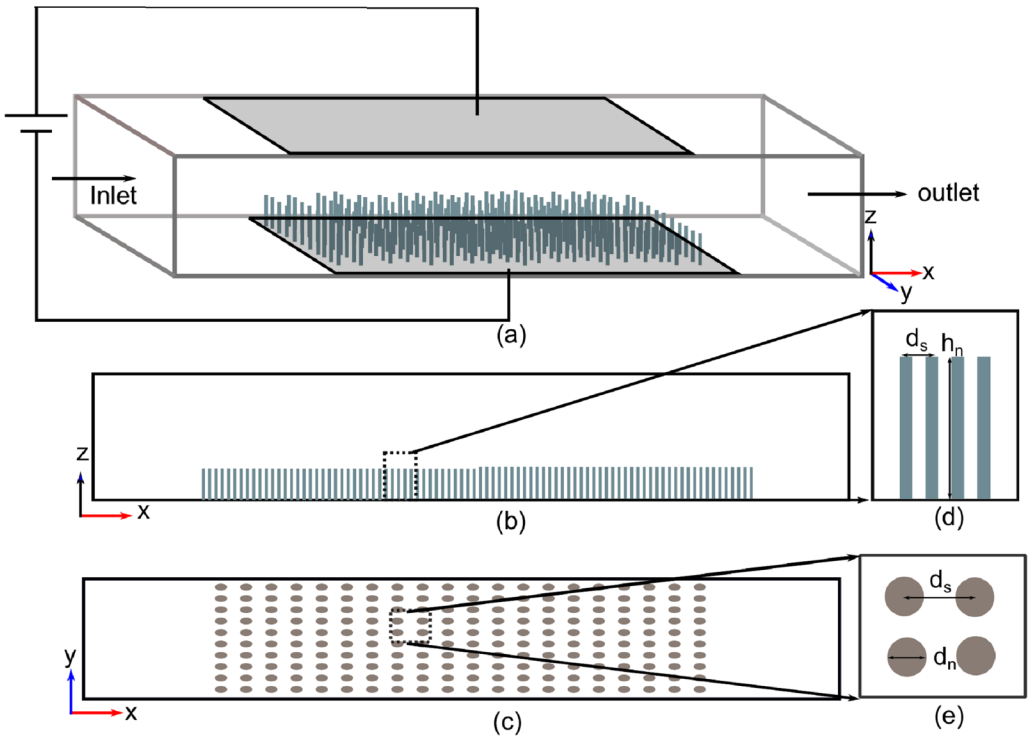

FIG. 1. (a) Illustration of a microfluidic channel containing nanowire array on the bottom (b) vertical cross section, (c) lateral cross section, (d) a repetitive unit on the vertical section of the channel, and (e) a repetitive unit on the lateral cross section of the channel. d_n, d_s, and h_n represent nanowire diameter, array spacing, and nanowire length, respectively.

semiconductor domain. The electric potential ϕ is related to the electric field as $E = -\nabla\phi$. The strain tensor is obtained by solving the stress equilibrium equation, which is given by

$$\nabla \cdot \sigma = 0, \quad \sigma = c\varepsilon - eE, \tag{2}$$

where σ and c are the stress tensor and the elastic tensor, respectively. The strain tensor is expressed as $\varepsilon = (\nabla u + \nabla u^T)/2$, where u is the displacement field. Charge density ρ_f in the fluid is the sum of ion density of the individual ion species and is given by $\rho_f = \sum_i z_i q a_i$, where z_i, and a_i are the valency and concentration of the ith ion species and q is the electronic charge. The charge density ρ_s in the nanowire is given by $-q(n - p + N_D^+ - N_A^-)$, where n (p) is the electron (hole) density and N_D^+ (N_A^-) is the ionized donor (acceptor) concentration. The details of computing the electron and hole densities due to coupled physical field interactions and quantum confinement in semiconductor nanostructures are explained in our earlier work.[42] In the fluid domain, the concentration a_i of the ith ion depends on the electric field and is governed by the Nernst–Planck equation that is given by

$$\nabla \cdot \left(-D_i \nabla a_i - \frac{D_i z_i q}{K_B T} a_i \nabla \phi \right) = 0, \tag{3}$$

where D_i is the diffusion coefficient of ith species, K_B is the Boltzmann constant, and T is the temperature. The dielectric permittivity tensor of the fluid also incorporates bound charges of the cells.[43] Furthermore, the charge concentration changes during lysis due to the release of intracellular components into the fluid. Here, we are mostly interested in steady-state conditions so that the temporal dependence of field variables are not considered.

Equations (1)–(3) should be solved simultaneously with appropriate boundary conditions. Any differential equation can be written as a weighted integral equation by multiplying a weight function and integrating over the domain. This has been explained in many finite element textbooks (for example, chapter 2 in Ref. 44). For building a finite element model, the set of differential equations should be written in the weighted integral form and then reduced to the variational/weak form by integrating by parts. The variational formulation for solving the problem using the finite element method can be posed as

$$\begin{aligned} &\int_{\Omega_s} \delta\phi(\nabla \cdot D - q[N_D^+ - n + p - N_A^-])d\Omega_s + \int_{\Omega_f} \delta\phi(\nabla \cdot D - \sum_\alpha z^\alpha q c^\alpha)d\Omega_f \\ &\int_{\Omega s} \delta u(\nabla \cdot \sigma)d\Omega_s + \sum_\alpha \int_{\Omega_f} \delta c^\alpha \nabla \cdot \left(-D_i \nabla a_i - \frac{D_i z_i q}{K_B T} a_i \nabla \phi \right) d\Omega_f = 0. \end{aligned} \tag{4}$$

The summation runs over the types of ions in the fluid medium. The applicable boundary conditions corresponding to Eq. (1) are either electric potential or charge density that should be specified on the boundaries. At the solid walls of the channel, electric potential has to be specified. At the channel inlet and outlet, the charge density should be specified. If we model a small repetitive unit block of the channel, the boundaries of the block are exposed to a constant electric field due to applied voltage. In such cases, we use a constant electric field on the boundaries parallel to the electrodes and periodic potential on the boundaries perpendicular to the field direction. At the solid/fluid interface, the stress normal to the solid is continuous whenever fluid–structure interactions are significant; otherwise, the stress-free boundary condition is used. At the channel inlet and outlet, either ion concentration or ion flux should be prescribed. At the electrodes, the ion flux is related to the current density. At solid surfaces other than electrodes, the ion flux vanishes.

B. Cell transport and probability of lysis in the microfluidic channel

Charged particles like biological cells present in the microfluidic channel experience force due to the non-uniform electric field distribution and fluid flow. The fluid flow in-turn is influenced by the electric field. For simplicity, we limit the present scope of modeling and simulation to the interaction between the nanowire and the electric field in the microfluidic channel. To the end of this study, the effect of the forces on the cells is estimated by considering the cells to be lumped masses. Furthermore, assuming the cell concentration to be small, the effect of particles on the field is negligible. Moreover, in the present case where we have a batch flow, the electric field is in the steady state and the fluid velocity is negligible. Hence, the drag force on the micro-scale particles such as bacterial cells is insignificant. However, for pulsed electric field, the force can become significant.

At any instant of time, the particle position x is obtained by

$$x(t) = \int_0^t v(t')dt' + x_0, \tag{5}$$

where x_0 represents the initial position of the particle, t is the time from initiation, and v is its velocity. The motion of a particle of mass m in a fixed frame of reference is governed by

$$F_E = \mathrm{m}\frac{\partial v}{\partial t}, \tag{6}$$

where F_E is the net force acting on the particle. The total force on a particle having radius a and zeta potential ζ_p can be written as the sum of electrophoretic and dielectrophoretic forces.[45] This is expressed as

$$F_E = 6\pi\zeta_p\epsilon_m E + 4\pi\epsilon_m a^3 K_{\mathrm{CM}} E\cdot\nabla E, \qquad K_{CM} = \frac{\epsilon_p - \epsilon_m}{\epsilon_p + 2\epsilon_m}, \tag{7}$$

where ϵ_m and ϵ_p are the dielectric permittivity of the medium and particle, respectively. K_{CM} is known as the Clausius–Mossotti (CM) factor.

The efficiency of the microfluidic channel in terms of lysing biological cells is estimated by computing a parameter defined by transport and lysis probability ($\mathrm{L_p}$). The probability of lysis of a cell under an electric field in the microfluidic channel is estimated as follows. Consider a cell moving along a path of length s. The total electric field intensity E_{tot} experienced by the cell during its trajectory is given by

$$\mathrm{L_p} = \begin{cases} 0, & \text{if } E_{tot} < E_{lt}, \\ 1, & \text{if } E_{tot} > E_{ut}, \\ 0.01 + \left(\dfrac{E_{tot} - E_{lt}}{E_{ut} - E_{lt}}\right)0.99, & \text{if } E_{lt} < E_{tot} < E_{ut}, \end{cases} \tag{8}$$

where E_{lt} (E_{ut}) is the lower (upper) threshold of electric field magnitude. If the total electric field magnitude experienced by a cell along its trajectory is below the threshold for it to undergo lysis, the cell remains intact. Hence, $\mathrm{L_p}$ is zero. If the field experienced is very high ($> E_{ut}$), then the cell gets lysed. In such cases, $\mathrm{L_p}$ is taken as 1. For intermediate field values, the factor $\mathrm{L_p}$ is calculated up to second-order accuracy. For $E_{tot} = E_{lt}$, $\mathrm{L_p} = 0.01$. For every $(0.01/0.99)(E_{ut} - E_{lt})$ increase in E_{tot} to E_{lt}, $\mathrm{L_p}$ increases by 0.01. Hence, for an intermediate value of E_{tot}, $\mathrm{L_p}$ is given by $0.01 + (E_{tot} - E_{lt}/E_{ut} - E_{lt})0.99$.

Here, we study the electrical lysis probability of channels considering *E. coli* cells as examples. The critical field required for *E. coli* lysis is 1 kV/cm,[18] which is chosen as the lower threshold. Based on the size and type of cells, an electric field of 0.6–2 kV/cm[46] is typically required for lysis of bacterial cells. A direct current (DC) of field strength typically in the range of 1–10 kV/cm[47] is required for lysis of prokaryotes or eukaryotes. Another design of microdevice reported a value of 1–10 kV/cm of field strength using pulsed alternating current (AC) for lysis of different variants of bacteria.[18] Therefore, an intermediate value (5 kV/cm) is chosen as the upper threshold. The mean of individual cell lysis probability gives the total lysis probability. Three repetitions were performed by releasing a different number of cells randomly in the simulation domain for statistical validation. The maximum number of cells released is always less than 0.5 times the simulation volume. In the present simulations, we neglect the effect of cells on the electric potential as the cell concentration is below 10^{14} cells/m^3. The simulations were carried out using COMSOL Multiphysics software. We have used the parallel sparse direct linear solver (PARDISO) to solve the numerical simulation problems.

III. RESULTS AND DISCUSSIONS

We investigate the effect of geometry, orientation, and inter-nanowire spacing on the electric field enhancement in the microfluidic channel. The semiconductor materials of nanowires are Si, SiO_2, and ZnO. ZnO is piezoelectric, whereas Si and SiO_2 are not piezoelectric and hence the piezoelectric terms in Eq. (2) can be neglected for Si and SiO_2 nanowires. So only the Eqs. (1) and (3) need to be solved simultaneously for the Si and SiO_2 nanowires. We consider a microfluidic channel configuration of dimension $10 \times 0.5 \times 0.5$ mm^3 (length × width × height). The spacing between the electrodes is 0.5 mm. The simulations are carried out for a repetitive unit in the microfluidic channel considering the two

TABLE I. Material parameters for wurtzite ZnO.

Material parameters	ZnO	Material parameters	ZnO
c_{11} (GPa)	209.7	c_{12} (GPa)	121.1
c_{13} (GPa)	105.9	c_{33} (GPa)	210.9
c_{44} (GPa)	105	P_{sp} (C/m^2)	−0.057
e_{15} (C/m^2)	−0.49	e_{31} (C/m^2)	−0.49
e_{33} (C/m^2)	0.73	ϵ_{33}	8.91
ϵ_{11}	7.77		

cases: (1) the plane perpendicular to the nanowire growth axis [Fig. 1(e)]; (2) the transverse plane containing the nanowire growth axis [Fig. 1(c)]. The fluid in the channel is assumed 1 mM phosphate-buffered saline (PBS) with dielectric permittivity of 75. Only the dominant ions (Na^+ and Cl^-) are considered with a diffusion coefficient of 1.033×10^{-9} m^2/s for Na^+[48] and 2.09×10^{-9} m^2/s for Cl^-.[49] For Si $\epsilon_r = 11.7$, and for SiO_2 $\epsilon_p = 3.9$.[50] The material parameters for ZnO[51] are tabulated in Table I. The nanowires are assumed to be 3 μm in length and 300 nm in diameter, and the inter-nanowire spacing is varied from 0.3 μm to 20 μm.

To quantify the effect of nanowire on the electric field in the microfluidic channel, we define the following parameters:

- Electric field enhancement factor (β_E) that gives the change in electric field intensity due to nanowires in the channel. It is defined as

$$\beta_E(x) = \frac{|E(x,t)|}{\phi_0/h},$$

which is the ratio of the magnitude of electric field intensity at x due to the presence of nanowire and magnitude of the applied electric field (ϕ_0/h). Here, ϕ_0 is the applied potential and h is the electrode gap in the channel. A value greater than 1 for β_E implies electric field amplification, whereas a value less than 1 implies electric field attenuation.

- The inter-nanowire spacing factor $D_s = d_n/d_s$ (Fig. 1).
- In the case of SiO_2 coated nanowires, if d_{n1} is the diameter of uncoated nanowire and d_{sh} is the SiO_2 shell thickness, then $C_s = d_{sh}/d_{n1}$ as shown in figure.
- In the case of ZnO nanowires, its pointedness is defined by angle α as shown in Fig. 5(b).

A. Lateral electric field interactions with a nanowire array

A horizontal cross section of the repetitive entity in the microfluidic channel with Si, SiO_2, and ZnO nanowires is shown in Figs. 2(a)–2(c), respectively, with the electric field applied along the y axis.

On these boundaries, a constant voltage is applied such that the voltage difference gives rise to an electric field of 1 kV/cm. To get an electric field of 1 kV/cm, we need an operational voltage of 50 V in the actual channel configuration. For the simulation domain, the voltage difference applied to maintain the same is in the range of 70 mV–700 mV for Ds varying from 0.9 to 0.1. On all the boundaries, we apply zero flux of ions for Eq. (3). Along the x axis, electric displacement consistent with zero flux condition is applied as the boundary condition. On the ZnO nanowire surfaces, we apply stress-free boundary conditions corresponding to the Eq. (2). The Si and SiO_2 nanowires have circular cross sections, whereas the ZnO nanowires have hexagonal cross sections. The magnitude of electric field distribution in the channel is shown in Figs. 3(a) and 3(b), respectively, for SiO_2 ($C_s = 1/3$) and ZnO ($\theta = 45°$) for $D_s = 0.4$.

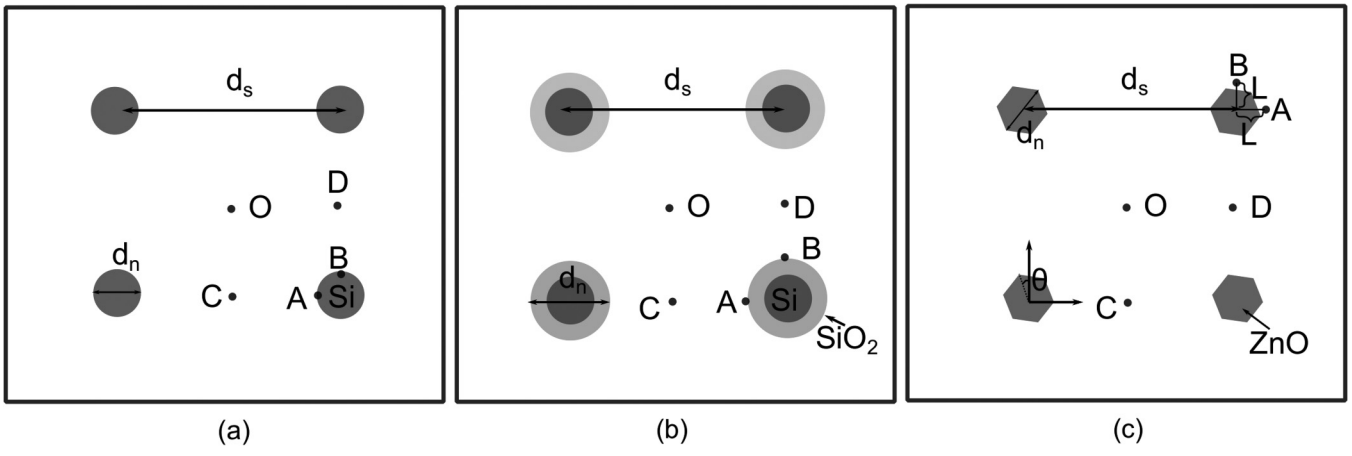

FIG. 2. Representative horizontal cross-sectional view of the microfluidic channel containing (a) Si, (b) SiO_2 coated Si, and (c) ZnO nanowire array. d_n and d_s depict the nanowire diameter and inter-nanowire spacing, respectively. L in (c) is equal to $d_n/2$. A, B, C, D, and O depict the positions where the electric field enhancement is calculated. The electric field enhancement in the channel for different inter-nanowire spacing is studied for all the three types of nanowires. Also, the effect of different SiO_2 coating thickness on electric field enhancement is studied in configuration (b). The effect of nanowire orientation to the applied electric field (indicated by θ) on the field enhancement is additionally studied in configuration (c).

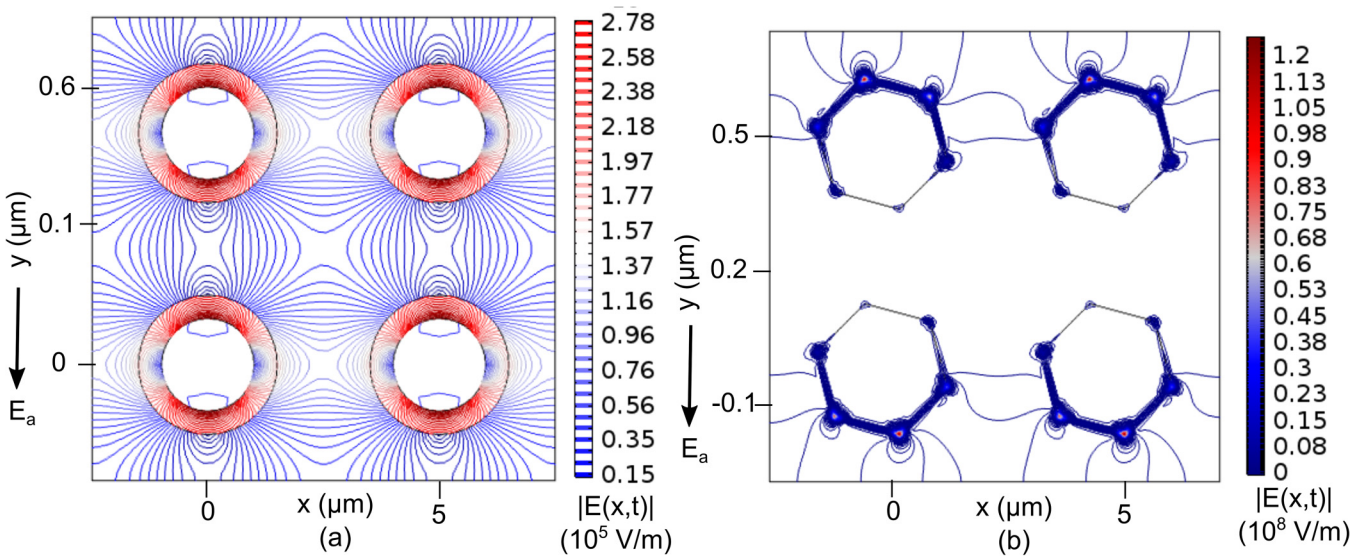

FIG. 3. Planar view of the electric field intensity (V/m) distribution in the microfluidic channel containing (a) Si–SiO_2 (C_s = 1/3) and (b) ZnO (θ = 45°) nanowire array with the inter-nanowire spacing factor, D_s = 0.4. E_a represents the direction along which the electric field is applied. The color bar represents the electric field intensity in V/m.

As seen in Figs. 3(a) and 3(b), the electric field gets localized near nanowires. As a result, the field is amplified in some regions and reduced in other regions surrounding the nanostructure, thus creating a non-uniform field distribution in the microfluidic channel. The presence of the Debye layer at the solid/fluid interface influences the electric field and field localization pattern. Observation on flat boundaries shows Debye length scales, which are much smaller than the micrometer length scale shown in Fig. 3. However, in non-smooth boundaries, it is not straightforward to compute the Debye length scale without detailed physical factors included in the simulations. Also there is an inter-nanowire screening effect present in the contours shown in Fig. 3. We have revisited some of the factors as follows. The structure of the Debye layer is influenced by the physical/chemical adsorption, orientation of dipoles, or chemical reaction between the solids and species in the fluid. This depends on several factors such as surface structure of the semiconductor, the nature of reactants in the fluid region, solvent molecules, etc. These are governed by reaction kinetics, charge transfer mechanisms at the semiconductor/fluid interfaces, electro-kinetic phenomena in fluids, etc. We have not considered the adsorption effect. Other effects described above are included. Adsorption effects need to be additionally considered along with Poisson's equation and coupling with the charge equations. Parameters required for the semiconductors for simulating this is not available and hence not studied. This can be either obtained from experiments or first principle studies. In the case of the Si and SiO_2 nanowires, the field is perturbed only close to nanowire surfaces. But in the case of ZnO nanowires, perturbations are spread throughout the channel as seen from the contour plot of the electric field in Fig. 3(b). Figures 2(a)–2(c) show the points where β_E is calculated. The vertices of the hexagon have a weak singularity in the electric field. For the electric field magnitude at these points, we chose the values of the fields at distance $d_n/2$ or $d_s/2$, whichever is closest to that point.

The variation of β_E with D_s for different C_s and θ are shown in Figs. 4(a)–4(j).

Higher enhancement is observed for channels with ZnO nanowires with nearly 30 times that of the applied field for θ = 45° orientation close to the nanowires. SiO_2 coated nanowires with a better enhancement for intermediate coating thickness (C_s = 1/3) follow this. For channels with Si–SiO_2 nanowires, the field enhancement at point B is observed only for certain inter-nanowire spacing. For channels with ZnO nanowires, the field enhancement is observed only for large inter-nanowire spacing (D_s below 0.06) at the proximity of nanowires. At points in between the nanowires (C), the field enhancement increases for Si–SiO_2 as the nanowire packing increases. Whereas for channels with ZnO nanowires, the field enhancement at C, D, and O are very high only for closely packed nanowires (D_s greater than 0.6). At points D and O, the field is attenuated by Si–SiO_2 nanowires with lower attenuation for large inter-nanowire spacing. However, at point D, the field is slightly enhanced by ZnO up to D_s = 0.06, after which there is attenuation up to D_s = 0.06. The orientation effects of ZnO nanowires on β_E is significant only for closely packed nanowires (D_s greater than 0.6) with maximum enhancement by ZnO arrays oriented at θ = 45°.

SiO_2 coated nanowires amplify the field better than non-coated ones due to the low permittivity of SiO_2. Permittivity is a measure of the amount of electric flux generated per unit charge in the medium. The lower the permittivity, the higher the electric flux and hence better the enhancement. However, in the case of ZnO, its unique geometry, as well as the piezoelectric reaction, leads to better amplification of the electric field. The effect of nanowire tips on field enhancement is studied next.

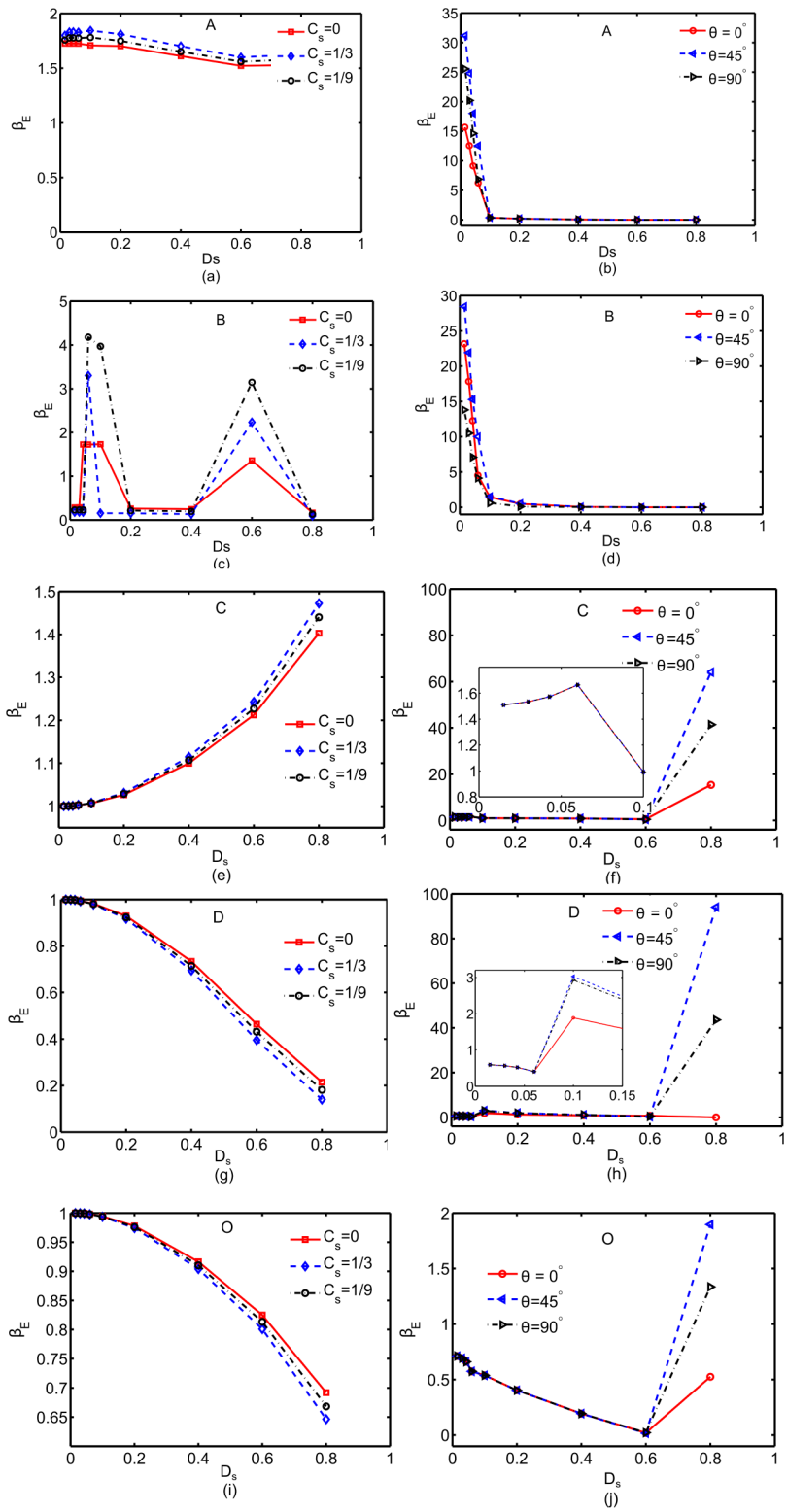

FIG. 4. Variation of field enhancement factor β_E with array spacing factor (D_s) for Si–SiO_2 nanowires for different SiO_2 shell thicknesses (C_s) at points (a) A, (c) B, (e) C, (g) D, and (i) O. Similarly, the variation of β_E with D_s for ZnO nanowires with different orientations (θ) to the applied electric field at points (b) A, (d) B, (f) C, (h) D, and (j) O. The points where the electric field enhancement is calculated are shown in Fig. 2.

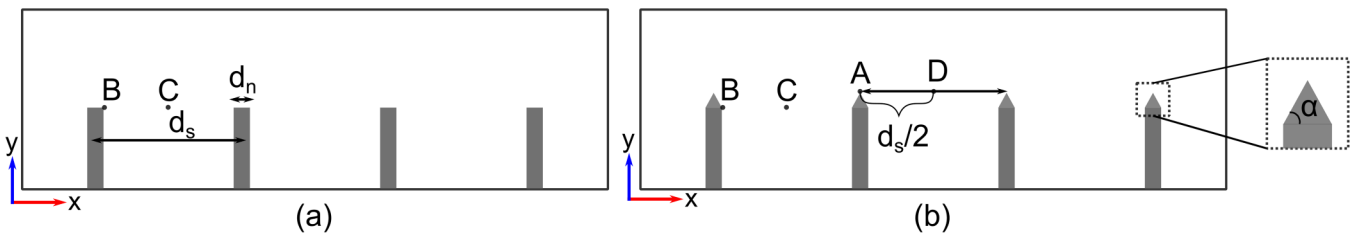

FIG. 5. Illustration of the vertical cross-sectional view of the microfluidic channel containing (a) Si and (b) ZnO nanowire arrays. The points A, B, C, and D represent the positions where the electric field enhancement is calculated. d_n, h_n, and d_s depict the nanowire diameter, height, and inter-nanowire spacing, respectively. The effect of inter-nanowire spacing is studied in all the configurations. Similar to the lateral cross section, the effect of SiO_2 thickness is additionally studied in configuration (a). The effect of nanowire pointedness (α) on field enhancement is also studied in configuration (b).

B. Transverse electric field interaction with a nanowire array

We investigate here the electric field concentration in the transverse plane cutting along the growth axis (*z* axis) of the nanowire along with the depth of the nanowire. A vertical cross section of a unit cell of the microfluidic channel is shown in Fig. 5.

The electric field is applied opposite to the nanowire growth direction. On these boundaries, a constant voltage giving rise to an electric field of 1 kV/cm is applied as the boundary conditions to the Eq. (1). For the simulation domain across the vertical cross section, the voltage difference applied to maintain the electric field of 1 kV/cm is 750 mV. On all boundaries, we apply zero flux of total ions as boundary conditions for Eq. (3). Along the *x* axis, an

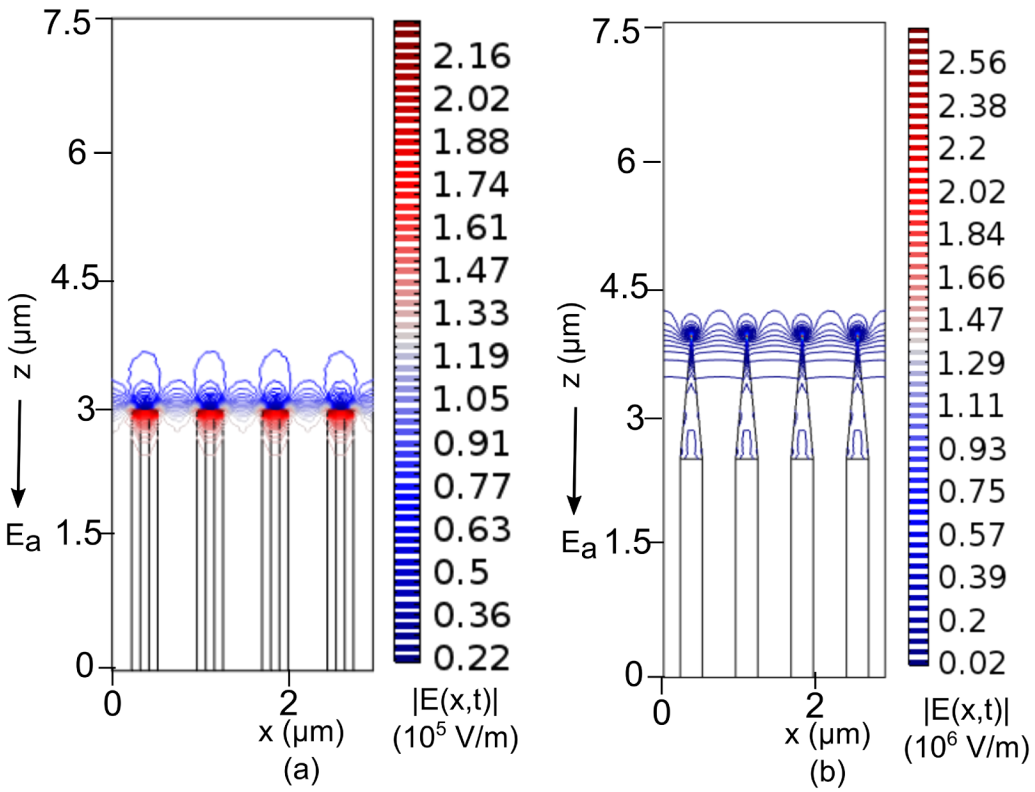

FIG. 6. Transverse planar view of the electric field magnitude (V/m) distribution in the microfluidic channel containing (a) Si–SiO_2 (C_s = 1/3) and (b) ZnO (α = 85°) nanowire array under an applied electrostatic field. E_a represents the direction along which the electric field is applied. The color bar represents the electric field intensity in V/m.

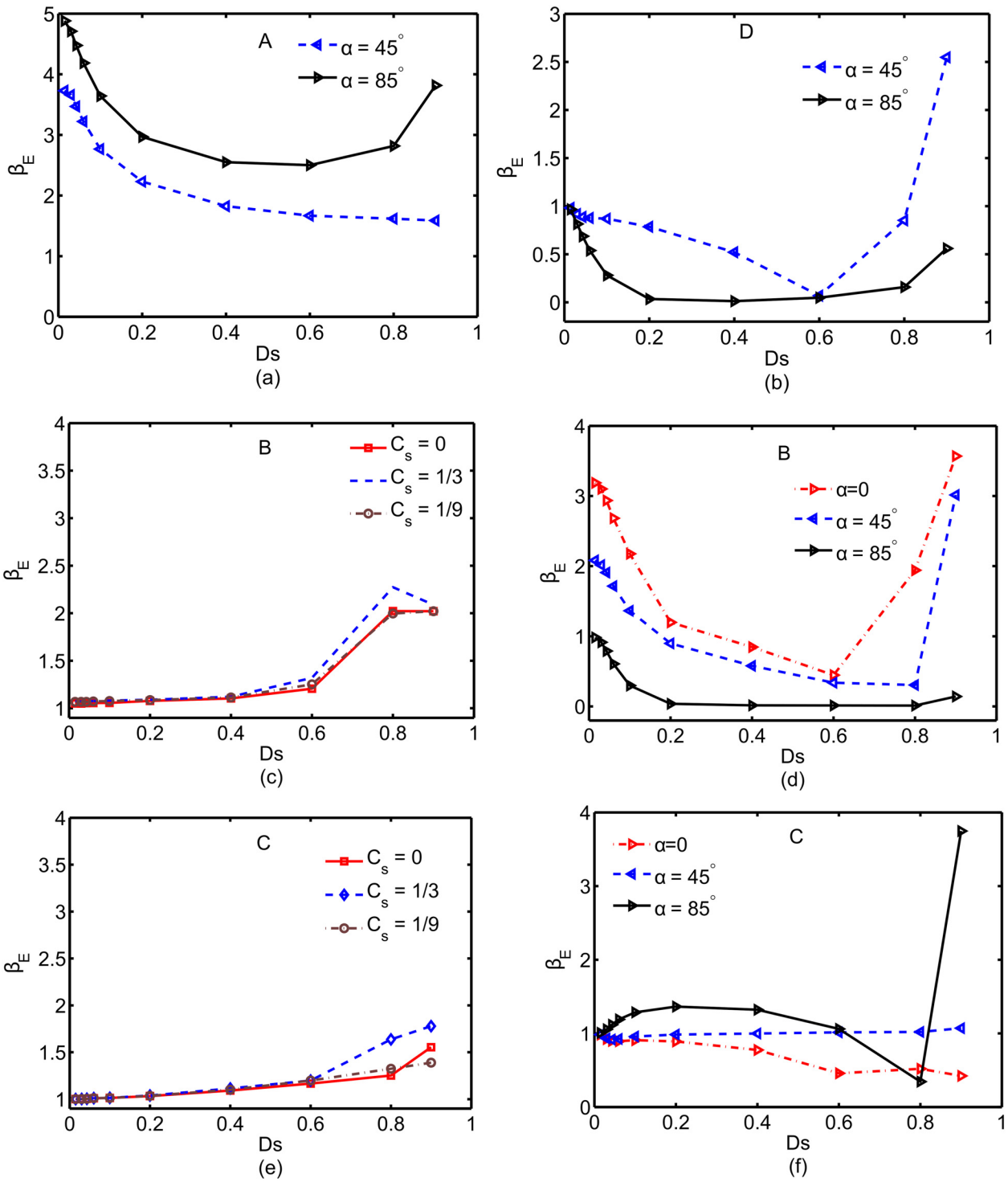

FIG. 7. Variation of electric field enhancement (β_E) with array spacing (D_s) for Si–SiO_2 nanowire for various SiO_2 coating thickness (C_s) at points (c) B and (e) C. Variation of β_E for channels with ZnO nanowire array having various pointedness (α) at points (a) A, (b) D, (d) B, and (f) C. The points where the electric field enhancement is calculated is shown in Fig. 5.

electric displacement consistent with zero flux is applied for Eq. (1). The ZnO nanowire surfaces are stress-free.

The electric field localization due to nanowires in the microfluidic channel is shown in Fig. 6(a) for SiO_2 ($C_s = 1/3$) and Fig. 6(b) for ZnO ($\alpha = 85°$) with $D_s = 0.4$.

As seen from Fig. 6(d), the electric field gets highly concentrated at the nanowire tips. Various points where β_E is calculated in the microfluidic channel is shown in Fig. 5. The points A and D, which are at the nanowire tip and in between the nanowire tips, are relevant only to ZnO nanowires with pointed tips. There are weak singularities at the tips and corners of the flat tips of nanowires. The electric field at these singular points is calculated as described earlier in Sec. III A.

Figures 7(a)–7(f) depict the variation of β_E with D_s for different C_s and α.

Similar to the lateral cross section, higher enhancement is observed in channels due to ZnO in comparison to Si–SiO_2 nanowires. The field enhancement due to Si–SiO_2 nanowires is nearly independent of nanowire spacing up to $D_s = 0.4$, beyond which it increases slightly with the highest enhancement for intermediate SiO_2 coating thickness. In channels with ZnO nanowires, maximum field enhancement is observed at the tips which increase with its pointedness. Additionally, higher enhancement is observed for largely spaced nanowires. The field attenuates steeply with the decrease in nanowire spacing at points in between the nanowire tips (point D) for sharper (larger α) nanowires. At point B, field enhancement is observed below $D_s = 0.02$ due to nanowires with $\alpha = 0°$ and 45°, whereas the field is attenuated due to nanowires with $\alpha = 85°$. Beyond this, the field is attenuated at this point irrespective of nanowire pointedness. However, the field is enhanced again for closely packed nanowires. ZnO with $\alpha = 45°$ shows optimal performance in terms of field enhancement as it shows lower attenuation for all D_s. For channels with the Si and SiO_2 nanowires, the field enhancement is slightly better for intermediate coating thickness of SiO_2 similar to observations in the horizontal plane. The combined effect of the pointed geometry, piezoelectric, and spontaneous polarization is responsible for enhancing the electric field in the case of channels with the ZnO nanowire array in this plane.

A previous design of micro-channel with the carbon nanotube array yielded a field enhancement of 10[52] with nanowires having the present aspect ratio. A design with geometrical modifications amplified the electric field 10 times at the orifice of constriction.[17] However, using the present design, the enhancement is 30 times using the ZnO nanowire array in the plane perpendicular to the growth axis. This means that the present configuration can effectively reduce the operating voltage required for biological cell lysis. This has an additional advantage of reducing bubble formation in the channel without compromising the generation of a high electric field. An estimate of the lysis efficiency of the channel is carried out in Sec. III C.

C. Cell transport and the probability of lysis in the microfluidic channel

Probabilistic evaluation of transport and lysis is important to understand the role of interaction on charged particles like

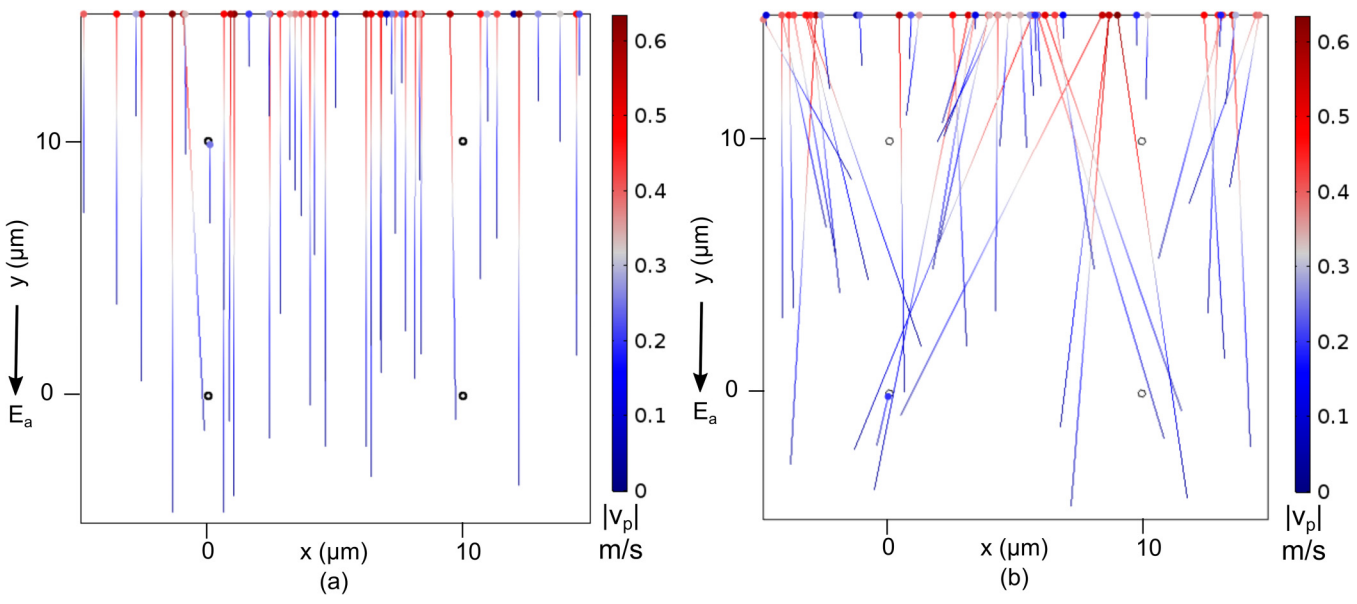

FIG. 8. *E. coli* motion trajectories in the microfluidic channel for lateral cross section under an applied electric field (E_a) of 1 kV/cm containing (a) Si–SiO_2 ($C_s = 1/3$) and (b) ZnO ($\theta = 45°$) nanowire array with array spacing equal to 10 μm at the end of 1 ms. The color bar represents the velocity magnitude of the cells. The solid circles denote the final position of the cell and the colors of the circle denote the velocity magnitude at the final position. The other end of the trajectory depicts the initial positions of the cells.

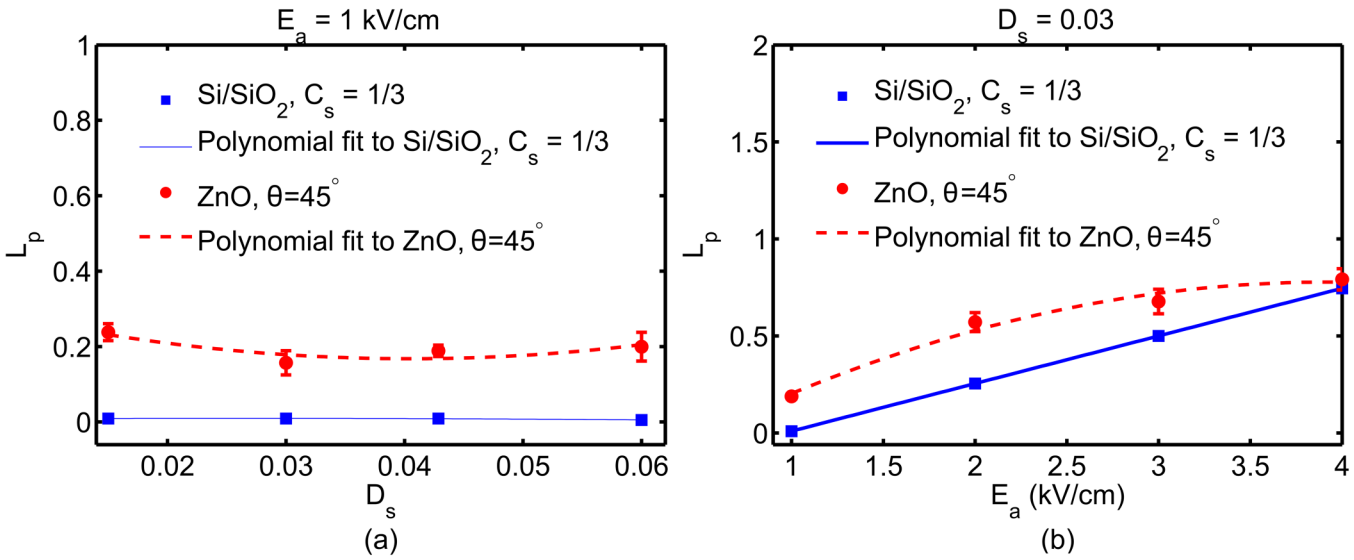

FIG. 9. Variation of transport and lysis probability (L_p) of *E. coli* cells in the microfluidic channel with (a) inter-nanowire spacing and (b) applied electric field. The values of the constants for the polynomial fit to the simulated data are tabulated in Table II.

biological cells present in the microfluidic channel with electric field distribution due to the nanowire array. The effectiveness of channels containing a nanowire in terms of lysing bacterial cells is studied in the present section for inter-nanowire spacing between 5 μm and 20 μm. We model the trajectories of spherical particles with a 1 μm radius assumed to have the properties of *E. coli* cells. The relative dielectric permittivity, mass density, and zeta potential are 12,[53] 1160 kg/m^3, and −40 mV,[54] respectively. The trajectories of *E. coli* cells at the end of 1 ms in the microfluidic channel containing SiO_2 ($C_s = 1/3$) and ZnO ($\theta = 45°$) are shown in Figs. 8(a) and 8(b), respectively, under 1 kV/cm applied electric field.

The final positions of the cells are shown with circles and the color bar shows the magnitude of particle velocity in units of m/s along its trajectory. The particles are initially located at the other end of the trajectories. We assumed that the cells freeze (retains its velocity) at the nanowire and simulation boundaries. We observe that the *E. coli* trajectory is greatly perturbed in the case of ZnO nanowire arrays, whereas SiO_2 has very little influence and almost all the cells get deposited on the electrodes. However, in the case of ZnO nanowire array, few cells are pushed toward the direction perpendicular to the applied electric field.

For quantitative purposes, we estimate the transport and lysis probability (L_p) to estimate the efficiency of the microfluidic channel. Figures 9(a) and 9(b) depict the variation of L_p with D_s and applied electric field (E_a), respectively.

L_p of cells in channels containing the ZnO nanowire array is greater than SiO_2 for all cases. A polynomial fit $a_1 D_s^2 + a_2 D_s + a_3$ and $b_1 E_a^2 + b_2 E_a + b_3$ to the simulated data are tabulated in the Table II. From Table II, it is observed that L_p decreases quadratically with D_s, whereas it increases linearly with E_a for SiO_2 nanowires but quadratically for ZnO nanowires. For very high electric fields, L_p of Si-based nanowire approaches that of ZnO nanowire arrays.

Similar calculations were made for vertical cross sections of the channels. Figures 10(a) and 10(b) show particle trajectories for channels with SiO_2 ($C_s = 1/3$) and ZnO ($\alpha = 45°$) nanowire arrays, respectively.

Similar to the horizontal cross section, we see that most of the cells deposit on the electrode for channels with SiO_2 nanowire array. In the case of channels with ZnO nanowire array, cells are scattered in all directions. The cells that are close to the nanowires are pushed in the direction perpendicular to the field direction. The variation of L_p with D_s and E_a are shown in Figs. 11(a) and 11(b), respectively.

L_p for channels with ZnO nanowire array is greater than SiO_2 for all cases. Furthermore, L_p varies linearly with D_s and E_a for channels with Si–SiO_2. For channels with ZnO, L_p varies

TABLE II. Fitting parameters for transport and lysis probability, L_p, of *E. coli* cells in microfluidic channels containing Si–SiO_2 and ZnO nanowires for lateral cross section vs inter-nanowire spacing factor, D_s, and applied electric field, E_a. The polynomial fits are represented by $a_1 D_s^2 + a_2 D_s + a_3$ and $b_1 E_a^2 + b_2 E_a + b_3$, respectively.

	a_1	a_2	a_3	b_1	b_2	b_3
Si–SiO_2	−3.6411	0.1921	0.0071	…	0.2453	0.2360
ZnO	98.1452	−7.9501	0.3287	−0.0671	0.5270	−0.25719

quadratically with D_s but linearly with E_a. The nature of the transport and lysis probability trend of micro-channels to D_s and E_a is linear in transverse cross section except for ZnO, which is quadratic to D_s. To consolidate, L_p of channels with a nanowire array decreases with the increase in D_s. Moreover, the lysis probability increases with the increase in the applied electric field. Furthermore, channels with ZnO nanowire array are better in lysing *E. coli* cells.

Polynomial fits $a_1D_s^2 + a_2D_s + a_3$ and $b_1E_a^2 + b_2E_a + b_3$ to the simulated data, similar to horizontal cross section, are tabulated in Table III.

Overall, the present design using semiconductor nanostructures is effective in amplifying the electric semiconductors that do not get corroded, unlike metal electrodes. This is because the metal electrodes tend to corrode easily when electrolytic fluids are used. The results show that *E. coli* cells are attracted to regions of

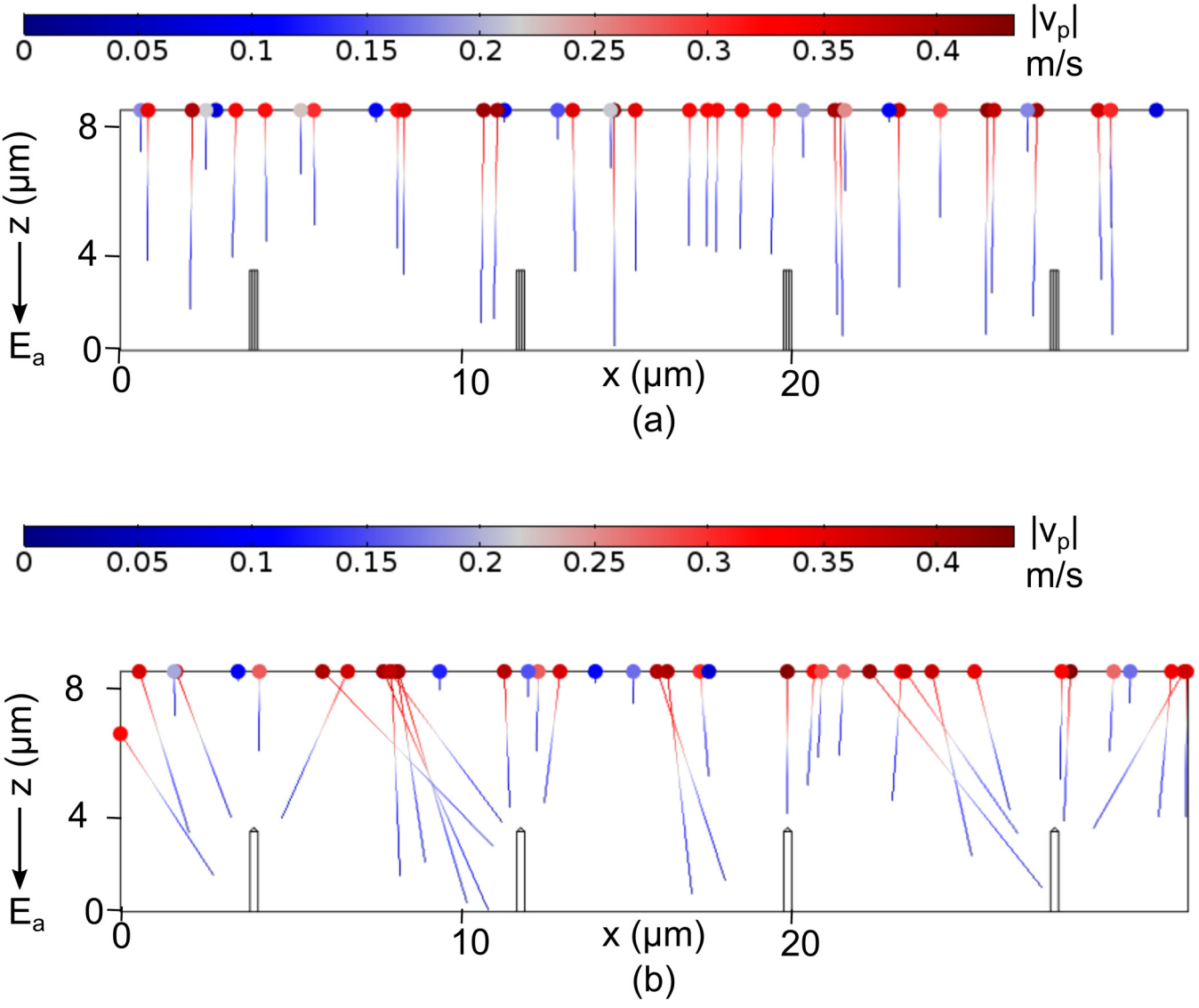

FIG. 10. *E. coli* motion trajectories in the microfluidic channel for transverse cross section under an applied electric field (E_a) of 1 kV/cm containing (a) Si–SiO_2 (C_s = 1/3) and (b) ZnO ($\theta = 45°$) nanowire array with array spacing equal to 10 μm at the end of 1 ms. The color bar represents the velocity magnitude of the cells. The solid circles denote the final positions of the cells and the colors of the circle denote the velocity magnitude at the final position. The other end of the trajectory depicts the initial positions of the cells.

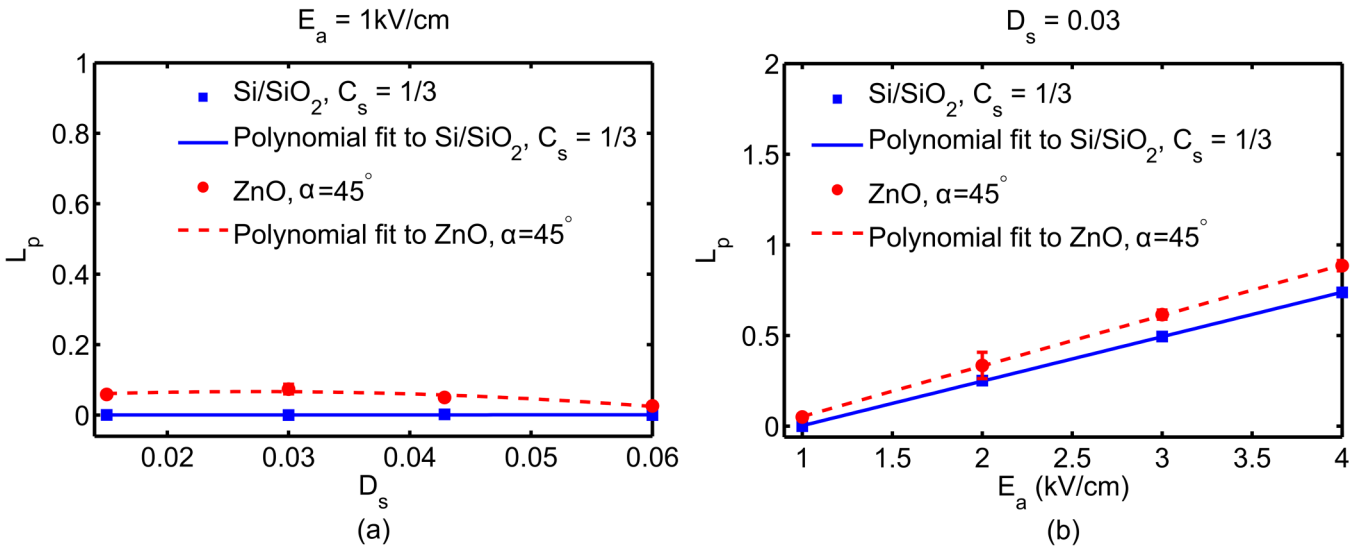

FIG. 11. Variation of transport and lysis probability of *E. coli* cells in the microfluidic channel with (a) inter-nanowire spacing and (b) applied electric field. The values of the constants for the polynomial fit to the simulated data are tabulated in Table III.

greater electric field strengths. The present model and simulation can help in understanding the role of nanowires in electric field distribution and its impact on the trajectories of micro-scale and nano-scale particles like bacteria for a better design. A simplified model was presented in Ref. 39 for estimating the field enhancement using CNT nanowires. In a previous design, electrodes of cuprous oxide carbon nanotubes on copper foam[37] proposed that the interaction between the nanowires and bacterial cells are the reason for disinfecting the water. With the carbon nanotubes on sponge,[38] a field enhancement of 1×10^7 V/m was estimated using simple analytical expressions. The model developed in the present study has diverse applications, independent of materials and geometry, and is more accurate in terms of obtaining electric field distribution. This can give better insights into future implementation of devices that involve nanostructure arrays for cell manipulation.

TABLE III. Fitting parameters for transport and lysis probability, L_p, of *E. coli* cells in microfluidic channels containing Si–SiO_2 and ZnO nanowires for transverse cross section vs inter-nanowire spacing factor, D_s, and applied electric field, E_a. The polynomial fits are represented by $a_1D_s^2 + a_2D_s + a_3$ and $b_1E_a^2 + b_2E_a + b_3$, respectively.

	a_1	a_2	a_3	b_1	b_2	b_3
Si–SiO_2	…	0.0058	0.0003	…	0.2454	−0.2430
ZnO	−39.1589	2.1252	0.0377	…	0.2787	−0.2256

IV. CONCLUSION

In conclusion, a microfluidic channel containing a semiconductor nanowire array for electrical cell lysis has been analyzed. We have studied the effect of nanowire geometry, size, and orientation on the electric field for the ZnO, Si, and SiO_2 arrays. The results show that such type of nanostructured microfluidic configuration using a semiconductor nanowire array is highly effective in amplifying the electric field strength. It is observed that for a given diameter to inter-nanowire separation ratio, the amplification of the electric field intensity in the case of ZnO nanowires is higher compared to that in the case of Si or SiO_2 nanowires. The combined effect of nanowire geometry, piezoelectric, and spontaneous polarization in a ZnO nanowire array is responsible for better enhancement. The optimum enhancement in ZnO is given by nanowires oriented at $\theta = 45°$ to the electric field in the plane perpendicular to the growth direction. The field enhancement at the nanowire tips increases as the pointedness increases. An intermediate coating thickness of SiO_2 yields better enhancement in comparison to non-coated nanowires. The effect of Si and SiO_2 nanowire is negligible on the trajectories of biological cells, whereas the ZnO nanowire array greatly influences the cell trajectories. The channels with the ZnO nanowire array have a greater probability of lysing cells. The lysis probability of the channel decreases as inter-nanowire spacing decreases except for ZnO in the vertical plane, whereas the lysis probability increases with the applied electric field.

ACKNOWLEDGMENTS

The authors acknowledge financial support from the Grand Challenge Canada Foundation through academic partner

subcontract Grant No. BIGT001 at the Indian Institute of Science and the industry partner Bigtec Labs Bangalore to carry out this research; D.R.M. acknowledges financial support from the Indo-German Science and Technology Centre (IGSTC) through project IDC-Water.

DATA AVAILABILITY

The data that support the findings of this study are available from the corresponding author upon reasonable request.

REFERENCES

[1]C. Prinz, J. O. Tegenfeldt, R. H. Austin, E. C. Cox, and J. C. Sturm, "Bacterial chromosome extraction and isolation," Lab Chip **2**(4), 207–212 (2002).
[2]J. W. Hong, V. Studer, G. Hang, W. F. Anderson, and S. R. Quake, "A nanoliter-scale nucleic acid processor with parallel architecture," Nat. Biotech. **22**(4), 435–439 (2004).
[3]P. C. H. Li and D. J. Harrison, "Transport, manipulation, and reaction of biological cells on-chip using electrokinetic effects," Anal. Chem. **69**(8), 1564–1568 (1997).
[4]P. Belgrader *et al.*, "A minisonicator to rapidly disrupt bacterial spores for DNA analysis," Anal. Chem. **71**(19), 4232–4236 (1999).
[5]J. Kim, S. Hee Jang, G. Jia, J. V. Zoval, N. A. Da Silva, and M. J. Madou, "Cell lysis on a microfluidic (CD) compact disc," Lab Chip **4**(5), 516–522 (2004).
[6]D. Di Carlo, K.-H. Jeong, and L. P. Lee, "Reagentless mechanical cell lysis by nanoscale barbs in microchannels for sample preparation," Lab Chip **3**(4), 287–289 (2003).
[7]L. C. Waters, S. C. Jacobson, N. Kroutchinina, J. Khandurina, R. S. Foote, and J. M. Ramsey, "Microchip device for cell lysis, multiplex PCR amplification, and electrophoretic sizing," Anal. Chem. **70**(1), 158–162 (1998).
[8]S. Baek, J. Min, and J.-H. Park, "Wireless induction heating in a microfluidic device for cell lysis," Lab Chip **10**(7), 909 (2010).
[9]J. El-Ali, S. Gaudet, A. Günther, P. K. Sorger, and K. F. Jensen, "Cell stimulus and lysis in a microfluidic device with segmented gas–liquid flow," Anal. Chem. **77**(11), 3629–3636 (2005).
[10]K. R. Rau, A. Guerra, A. Vogel, and V. Venugopalan, "Investigation of laser-induced cell lysis using time-resolved imaging," Appl. Phys. Lett. **84**(15), 2940–2942 (2004).
[11]K. R. Rau, P. A. Quinto-Su, A. N. Hellman, and V. Venugopalan, "Pulsed laser microbeam-induced cell lysis: Time-resolved imaging and analysis of hydrodynamic effects," Biophys. J. **91**(1), 317–329 (2006).
[12]J. Cheng *et al.*, "Preparation and hybridization analysis of DNA/RNA from E. coli on microfabricated bioelectronic chips," Nat. Biotech. **16**(6), 541–546 (1998).
[13]G. Mernier, N. Piacentini, T. Braschler, N. Demierre, and P. Renaud, "Continuous-flow electrical lysis device with integrated control by dielectrophoretic cell sorting," Lab Chip **10**(16), 2077–2082 (2010).
[14]H. Lu, M. A. Schmidt, and K. F. Jensen, "A microfluidic electroporation device for cell lysis," Lab Chip **5**(1), 23–29 (2005).
[15]H. Y. Wang, A. K. Bhunia, and C. Lu, "A microfluidic flow-through device for high throughput electrical lysis of bacterial cells based on continuous dc voltage," Biosens. Bioelectron. **22**(5), 582–588 (2006).
[16]N. Bao and C. Lu, "A microfluidic device for physical trapping and electrical lysis of bacterial cells," Appl. Phys. Lett. **92**, 214103 (2008).
[17]C. Church, J. Zhu, G. Huang, T. R. Tzeng, and X. Xuan, "Integrated electrical concentration and lysis of cells in a microfluidic chip," Biomicrofluidics **4**, 044101 (2010).
[18]S. W. Lee, H. Yowanto, and Y. C. Tai, "A micro cell lysis device," in *The Eleventh Annual International Workshop on Micro Electro Mechanical Systems, 1998, MEMS 98* (IEEE, 1998), pp. 443–447.
[19]M. A. McClain, C. T. Culbertson, S. C. Jacobson, N. L. Allbritton, C. E. Sims, and J. M. Ramsey, "Microfluidic devices for the high-throughput chemical analysis of cells," Anal. Chem. **75**(21), 5646–5655 (2003).
[20]D. W. Lee and Y. Cho, "A continuous electrical cell lysis device using a low dc voltage for a cell transport and rupture," Sens. Actuators B Chem. **124**(1), 84–89 (2007).
[21]B. L. Hogan and E. S. Yeung, "Determination of intracellular species at the level of a single erythrocyte via capillary electrophoresis with direct and indirect fluorescence detection," Anal. Chem. **64**(22), 2841–2845 (1992).
[22]Q. Xue and E. S. Yeung, "Determination of lactate dehydrogenase isoenzymes in single lymphocytes from normal and leukemia cell lines," J. Chromatogr. B Biomed. Sci. Appl. **677**(2), 233–240 (1996).
[23]J. Gao, X.-F. Yin, and Z.-L. Fang, "Integration of single cell injection, cell lysis, separation and detection of intracellular constituents on a microfluidic chip," Lab Chip **4**(1), 47–52 (2004).
[24]R. C. Lee *et al.*, "Biophysical mechanisms of cell membrane damage in electrical shock," Semin. Neurol. **15**(4), 367–374 (1995).
[25]K. R. Rostgaard *et al.*, "Vertical nanowire arrays as a versatile platform for protein detection and analysis," Nanoscale **5**, 10226 (2013).
[26]H. J. Yoon, M. Kozminsky, and S. S. Nagrath, "Emerging role of nanomaterials in circulating tumor cell isolation and analysis," ACS Nano **8**(3), 1995–2017 (1998).
[27]G. Zheng, F. Patolsky, Y. Cui, W. U. Wang, and C. M. Lieber, "Multiplexed electrical detection of cancer markers with nanowire sensor arrays," Nat. Biotechnol. **23**(10), 1294–1301 (2005).
[28]M. Lin *et al.*, "Nanostructure embedded microchips for detection, isolation, and characterization of circulating tumor cells," Acc. Chem. Res. **47**, 2941–2950 (2014).
[29]C. Wang *et al.*, "Simultaneous isolation and detection of circulating tumor cells with a microfluidic silicon-nanowire-array integrated with magnetic upconversion nanoprobes," Biomaterials **54**, 55–62 (2015).
[30]D. P. Nevelinga, T. S. van den Heever, W. J. Perold, and L. M. T. Dicks, "A nanoforce ZnO nanowire-array biosensor for the detection and quantification of immunoglobulins," Sens. Actuators B Chem. **203**, 102–110 (2014).
[31]G.-J. Zhang and Y. Ning, "Silicon nanowire biosensor and its applications in disease diagnostics: A review," Anal. Chim. Acta **749**, 1–15 (2012).
[32]T. Berthing *et al.*, "Cell membrane conformation at vertical nanowire array interface revealed by fluorescence imaging," Nanotechnology **23**, 415102 (2012).
[33]A. A. Tahrim, A. Ahmad, and M. S. M. Ali, "A review on the potential of silicon nanowires (sinws) in thermoelectric energy harvesters," J. Teknol. **77**(17), 11–17 (2015).
[34]M. Koto, P. W. Leu, and P. C. McIntyre, "Vertical germanium nanowire arrays in microfluidic channels for charged molecule detection," J. Electrochem. Soc. **156**(2), K11–K16 (2009).
[35]X. Liu and S. Wang, "Three-dimensional nano-biointerface as a new platform for guiding cell fate," Chem. Soc. Rev. **43**(8), 2385–2401 (2014).
[36]J. Kim, J. W. Hong, D. P. Kim, J. H. Shin, and I. Park, "Nanowire-integrated microfluidic devices for facile and reagent-free mechanical cell lysis," Lab Chip **12**(16), 2914–2921 (2012).
[37]Z. Y. Huo, X. Xie, T. Yu, Y. Lu, C. Feng, and H. Y. Hu, "Nanowire-modified three-dimensional electrode enabling low-voltage electroporation for water disinfection," Environ. Sci. Technol. **50**(14), 7641–7649 (2016).
[38]Z. Y. Huo *et al.*, "Carbon-nanotube sponges enabling highly efficient and reliable cell inactivation by low-voltage electroporation," Environ. Sci. Nano **4**(10), 2010–2017 (2017).
[39]Z. Y. Huo *et al.*, "Cell transport prompts the performance of low-voltage electroporation for cell inactivation," Sci. Rep. **8**(1), 1–10 (2018).
[40]J. Kim, Z. Li, and I. Park, "Direct synthesis and integration of functional nanostructures in microfluidic devices," Lab Chip **11**(11), 1946–1951 (2011).
[41]R. Vasireddi, B. Javvaji, H. Vardhan, D. R. Mahapatra, and G. M. Hegde, "Growth of zinc oxide nanorod structures: Pressure controlled hydrothermal process and growth mechanism," J. Mater. Sci. **52**, 2007–2020 (2017).

[42]B. M. Shenoy, D. R. Mahapatra, and G. Hegde, "A model of coupled thermal, mechanical, and electrostatic field effects in III-N thin film heterostructures," J. Appl. Phys. **114**(4), 44506 (2013).
[43]G. H. Markx and C. L. Davey, "The dielectric properties of biological cells at radiofrequencies: Applications in biotechnology," Enzyme Microb. Technol. **25**(3–5), 161–171 (1999).
[44]J. N. Reddy, "Integral formulation and variational methods," in *An Introduction to the Finite Element Method*, 2nd ed., edited by J. J. Corrigan and J. M. Morriss (McGraw-Hill, 1993), pp. 18–35.
[45]T. B. Jones, "Basic theory of dielectrophoresis and electrorotation," IEEE Eng. Med. Biol. Mag. **22**, 33–42 (2003).
[46]M. S. Islam, A. Shahid, K. Kuryllo, Y. Li, M. J. Deen, and P. R. Selvaganapathy, "Electrophoretic concentration and electrical lysis of bacteria in a microfluidic device using a nanoporous membrane," Micromachines **2**, 45 (2017).
[47]H. Y. Wang, P. P. Banada, A. K. Bhunia, and C. Lu, "Rapid electrical lysis of bacterial cells in a microfluidic device," Methods Mol. Biol. **385**, 23–35 (2007).
[48]X. Y. Chen, K. C. Toh, J. C. Chai, and C. Yang, "Developing pressure-driven liquid flow in microchannels under the electrokinetic effect," Int. J. Eng. Sci. **42**, 609–622 (2004).
[49]S. Qian, B. Das, and X. Luo, "Diffusioosmotic flows in slit nanochannels," J. Colloid Interface Sci. **315**, 721–730 (2007).
[50]P. R. Gray, P. J. Hurst, S. H. Lewis, and R. G. Meyer, *Analysis and Design of Analog Integrated Circuits*, 4th ed. (Wiley, 2001).
[51]H. Morkoç and Ü. Özgür, *Zinc Oxide Fundamentals, Materials and Device Technology* (Wiley-VCH, 2009).
[52]J. A. Rojas-Chapana, M. A. Correa-Duarte, Z. Ren, K. Kempa, and M. Giersig, "Enhanced introduction of gold nanoparticles into vital acidothiobacillus ferrooxidans by carbon nanotube-based microwave electroporation," Nano Lett. **4**(5), 985–988 (2004).
[53]W. Bai, K. S. Zhao, and K. Asami, "Dielectric properties of E. coli cell as simulated by the three-shell spheroidal model," Biophys. Chem. **122**(2), 136–142 (2006).
[54]K. A. Soni, A. K. Balasubramanian, A. Beskok, and S. D. Pillai, "Zeta potential of selected bacteria in drinking water when dead, starved, or exposed to minimal and rich culture media," Curr. Microbiol. **56**(1), 93–97 (2008).